Arabian Journal for Science and Engineering (2024) 49:9611–9624
https://doi.org/10.1007/s13369-024-08903-z

RESEARCH ARTICLE-CHEMISTRY

Synergistic Effects of Carbon Nanotubes (CNTs) and White Graphite (h-BN) on the Microstructure and Mechanical Properties of Aluminum Matrix Composites

Muhammad Awais Khan[1] · Atteeq Uz Zaman[1] · Khurram Imran Khan[1] · Muhammad Ramzan Abdul Karim[1] · Azhar Hussain[2] · Ehsan ul Haq[3]

Received: 25 October 2023 / Accepted: 19 February 2024 / Published online: 3 April 2024

Abstract

The increased demand for lightweight structural materials in the transport sector has compelled researchers to develop materials with high strength and reduced structural weight, aiming to enhance vehicle performance, minimize fuel and oil consumption and reduce CO_2 emissions. However, their structural weight and strength still need to be improved. Herein, an attempt has been made to fabricate aluminum-based composites reinforced with hexagonal boron nitride (h-BN: 1,3,5,7 wt%) and multi-walled carbon nanotubes (MWCNTs: 0.25, 0.5, 0.75, 1 wt%) through powder processing method. The results revealed that the 3BN/Al composite disclosed better densification (96.8%) and hardness (49 $\pm$ 1.5) among all BN/Al composites. Furthermore, the addition of 0.5 wt% CNTs to BN/Al composite significantly improved the densification (97.7%), Vickers hardness (106%) and tensile strength (189%) over pure Al. This improvement was attributed to homogeneously distributed h-BN and CNTs in the Al matrix and the formation of hard aluminum carbide (Al_4C_3) phase. The results demonstrate that BN/CNTs/Al composite exhibits superior mechanical strength, making them promising structural and functional materials for aerospace and automobile industries.

Keywords Aluminum matrix composites · White graphite · Carbon nanotubes · Mechanical properties · Microstructure

1 Introduction

Metal matrix composites have gained prominence and sparked a lot of research interest due to the need and significance of lightweight and high-specific strength materials. Owing to their peculiar properties of being lightweight and better mechanical strength [1], nowadays, MMCs are used as alternatives to metallic components in a variety of applications such as aerospace, automobile and marine industries [2]. Ceramics or carbon-based materials are employed as reinforcement in MMCs to optimize the mechanical strength, elastic modulus, corrosion and wear resistance of the composite [3, 4].

In MMCs, magnesium, titanium, copper and aluminum are considered as the most preferable matrix materials. Aluminum, among all, is the most often utilized and researched metal, attributed to its lightweight, good machinability and excellent electrical and thermal properties particularly in aerospace and automobile industries [5, 6]. However, aluminum retains quite moderate mechanical properties (UTS 90 MPa, UCS 80 MPa, YS 30 MPa) which ought to be enhanced while preserving the benefit of being lightweight. The addition of a second phase (reinforcement) with superior mechanical properties and low density would increase the stiffness and strength of the matrix.

Muhammad Awais Khan and Atteeq Uz Zaman have contributed equally to this work.

✉ Muhammad Ramzan Abdul Karim
ramzan.karim@giki.edu.pk; ramzan1109@hotmail.com

Ehsan ul Haq
amonehsan@uet.edu.pk

[1] Faculty of Materials and Chemical Engineering, Ghulam Ishaq Khan Institute of Engineering Sciences and Technology, Topi 23640, Pakistan

[2] Department of Metallurgy and Materials Engineering, University of Engineering and Technology, Taxila 47050, Pakistan

[3] Department of Metallurgical and Materials Engineering, University of Engineering and Technology, Lahore 54890, Pakistan

Several researchers reported significant improvement in the mechanical properties of Al matrix composite by the inclusion of nitrides such as titanium nitride (TiN) [7], boron nitride (BN) [8] and aluminum nitride (AlN) [9]. For Al matrix composite, h-BN is considered an excellent reinforcement due to its low density, high hardness, high melting point and good wear and high impact resistance. Due to its outstanding properties, BN-reinforced Al composites are utilized for pistons, brake rotor, bearing surface and brake drums in automobile industries [10–14]. During the last decades, carbon nanotubes (CNTs) have drawn the attention of researchers as a reinforcement, owing to its remarkable mechanical and thermal properties such as low density (1.3–2 g/cm^3), high aspect ratio (100–1000) [15, 16], low coefficient of thermal expansion (CTE) [15, 16], exceptionally high Young modulus (~ 1.25 TPa) [17], high thermal conductivity (6600 W/mK) [18] and extremely high stiffness and strength (~ 30 GPa) [19, 20]. In recent years, the anticipated strength of materials reinforced by merely using carbon-based materials (CNTs, GNPs, graphite, etc.) or ceramic materials (SiC, Si_3N_4, AlN, ZrB_2, ZrO_2, etc.) has not been achieved. Thus, we propose a novel and synergistic approach for fabricating Al matrix composites, incorporating both carbon nanotubes and hexagonal boron nitride (h-BN) as reinforcements. Thus, aluminum matrix composite (BN-CNTs/Al) can be a promising option for achieving a good combination of desirable mechanical properties.

Numerous researchers have successfully evaluated the tribological and mechanical behavior of Al–CNTs, Al–ZrB_2, Al–SiC, Al–ZrO_2 and Al–BN composites separately. Bach et al. [21] aimed to investigate the influence of Mg and AlN composite Al alloy microstructure and electrochemical properties. They reported that the addition of Mg and AlN refined the grain size and improved resistance to pitting corrosion. Additionally, it enhanced charge transfer resistance and promoted stable passive film formation. Vinayagam et al. [22] reported mechanical performance of the Al alloy reinforced with various contents of AlN particles (0 to 12 wt%) fabricated through stir casting. The finding disclosed that composite with 12 wt% of AlN exhibited significantly enhanced hardness (40%), tensile strength (64%) and compressive strength (33%) as compared to monolithic alloy. Kumar et al. [23] have investigated the effect of ZrB_2 on the corrosion and mechanical properties of Al alloy and reported that with inclusion of 10 wt% of ZrB_2 improved the hardness, tensile strength and bending strength by 26%,15% and 26%, respectively, as compared to monolithic alloy. Vithal et al. [24] aimed to enhance mechanical properties and strengthening mechanism of A7075/ZrB_2 via stir casting. Their results revealed a significant improvement in hardness (29%), tensile strength (34%), yield strength (60%) and elastic modulus (23%) with inclusion of ZrB_2 as compared to base alloy.

Similarly, Bandil et al. [25] used SiC to enhance mechanical and corrosion properties of Al-Si alloy, indicating 15 wt% SiC improved hardness by 85% and protection efficiency by 56%. Rahman et al. [26] employed stir casting to fabricate Al matrix composite reinforced with SiC (0 to 20 wt. %) and Mg (1 wt%), revealing improved hardness and tensile strength. Particularly, 20 wt% SiC exhibited maximum enhancements, with a 175% increase in tensile strength and 87% in hardness. James et al. [27] studied the mechanical properties of the Al-reinforced ZrO_2 and Al_2O_3 prepared via stir casting. They reported that the incorporation of 5 wt% of ZrO_2 improved the hardness and tensile strength of the composite, reaching a value of 82.9 HV in hardness and 232 MPa in tensile strength. Kuldeep Pal et al. [28] utilized ZrO_2 nanoparticles (0-6wt%) to improve mechanical and corrosion properties of Al matrix via powder metallurgy. Al-6 wt% ZrO_2 enhanced the hardness by 9.57%, wear resistance by 63.91% and corrosion resistance efficiency by 70% compared to Al without reinforcement.

Ahmed et al. [29] reported that grain refinement and the inclusion of 0.1 wt% B and 0.5 wt% Ti modifiers significantly improved the mechanical properties of an Al–Mg alloy. They achieved a tenfold reduction in grain size and observed notable increases in hardness (18.8%), strain (100%) and tensile strength (30.5%) compared to the unmodified alloy. Kaygısız et al. [30] explored the effect of heat treatment on the corrosion and hardness of Al–Si–Mg alloy with different growth rates. An increase in hardness was observed with the influence of solution heat treatment and grain growth, while the corrosion resistance of the alloy was enhanced with high solidification and the application of heat treatment.

As for CNTs-reinforced aluminum matrix composites, Bosel et al. [31] fabricated Al-1 vol% CNTs composites through wet mixing followed by consolidation via SPS. The addition of CNTs leads to a notable increase in tensile strength (from 68 MPa to 95.5 MPa) and failure strain (from 3 to 5.5%). Pérez-Bustamante et al. [32] examined the impact of MWCNTs on the ultimate tensile strength and yield strength of the Al-based composite. They stated that the composite incorporation of 2 wt% of multi-walled CNT exhibited the maximum increment of ~ 95% and ~ 100% in ultimate tensile strength and yield strength, respectively, compared to pure Al. He et al. [33] successfully fabricated CNT/Al composite via in situ chemical vapor deposition and observed that the incorporation of 5 wt% CNTs to the composite significantly enhanced the elastic modulus and tensile strength by ~ 34% and ~ 180%, respectively. Guo et al. [34] reported the influence of various CNTs contents and sintering temperature on the CNTs/Al composites prepared via SPS and hot rolling. Optimal mechanical properties were achieved with 0.75 vol% CNTs/Al, reaching a value of 220 MPa in tensile strength, 200 MPa in yield strength and 21% in elongation, attributed

to the better interfacial bonding of CNTs and Al, equal dispersion of CNTs and improved densification. Zhang et al. [35] examined the impact of hybrid reinforcement (CNTs and SiC_p) on the mechanical strength and microstructure of CNT-SiC_p/Al composites. The results indicated that the composite having 0.5 CNT-0.5SiC_p/Al exhibited tensile strength enhanced by 94%, as compared to pure Al. Furthermore, the pinning action of SiC_p as scattered particles around the CNTs can prevent and prolong the peeling and pulling out of CNTs to further increase CNTs' strengthening effect. Panchal Reddy et al. [11] researched the impact of nano-BN on the thermal and mechanical strength of aluminum-based composites. Different h-boron nitride concentrations (0.5, 1.5, 2 vol.%) were utilized and observed that 1.5 vol.% of BN led to significant improvements in compressive strength (48.67%), hardness (83%) and tensile strength (32.77%) compared to pure Al. Gostariani et al. [36] examined the mechanical characteristics of Al-based nanocomposites with varying amounts of nano-BN reinforcement (1, 2 and 4 wt%). The results showed that the inclusion of 4 wt% BN to Al-BN nanocomposites led to significantly enhanced tensile strength (55%) and hardness (90%) compared to pure Al.

Although significant research has been conducted on the mechanical and microstructure behaviors of CNTs- or BN-reinforced Al composites separately, to the best of author's knowledge, there is room for evaluation of hybrid effects of both of these reinforcements (h-BN & CNTs) when added to Al matrix. The current work is a first try to explore the synergistic effects of white graphite (h-BN) and CNTs in the aluminum matrix on its physical and mechanical characteristics. h-BN having a unique layered structure like graphite and CNTs having exceptional mechanical properties can enhance the wear resistance and mechanical properties of aluminum or aluminum based matrices. Hence, the objective of this study is to fabricate Al matrix composites (BN/Al, 3BN-CNTs/Al) with various weight percent contents of BN (1, 3, 5, 7 wt%) and CNTs (0.25, 0.5, 0.75, 1 wt%) in order to evaluate the synergistic effects on the density, microstructure, hardness and tensile strength of the aluminum matrix composites for their potential applications in automotive and aerospace industry. Among the prepared compositions, BN-CNTs/Al composites exhibited optimal mechanical properties by the inclusion of 3 wt% BN and 0.5 wt% CNTs.

2 Experimental Procedure

2.1 Raw Materials

In this study, commercially available, raw aluminum powder (99% purity, median particle size ~ 1–2 μm, Sigma-Aldrich) was employed as matrix material. However, hexagonal boron nitride (particle size ~ 1 μm, ~ 99% purity, Liao ning peng Company Ltd, China) and MWCNTs (ID 5-15 nm, OD 50 nm, length of ~ 10–20 μm, Macklin) were used as reinforcements. The physical properties of the matrix and reinforcing materials are presented in Table 1.

Table 1 Properties of aluminum, h-BN and CNTs powders

Materials	Theoretical Density (g/cm^3)	Average particle size (μm)
Al	2.70	1–2
h-BN	2.30	≤ 1
CNTs	1.80	D = 50 nm, L = 10–20 μm

2.2 Methodology

Initially, the commercially available raw powder of Al and h-BN (1, 3, 5, 7 wt%) was weighted according to the compositions given in Table 2. After weighing powder, each composition of h-BN/Al was subjected to probe sonication for 1 h in ethanol solution. The resulting h-BN/Al mixture was subsequently ball-milled for 12 h at 150 rpm to obtain the homogeneous blend. The prepared mixture was then placed in oven for 20 h at 70 °C to remove any residual moisture. The dried powders were then compacted into different shapes cylindrical pellets of dimension (3 mm thickness and 12 mm dia) and rectangular bar of dimension (35 × 10 × 3 mm) using uniaxial pressing at 500 MPa pressure for 3 min. The green samples were conventionally sintered in a tube furnace at 630 °C with a heating rate of 10 °C/min for 180 min under controlled environment of argon. The sintered specimens were then ground using SiC abrasive paper with the grid size varying from 320 to 4000. Finally, the grounded specimens were fine polished with a micro cloth along with 0.25 μm diamond paste. The best composition among h-BN/Al based on physical and mechanical properties was then utilized to synthesize BN-CNTs/Al composites. For the fabrication of BN-CNTs/Al composites, a specific reinforcing proportion of h-BN (3 wt%) and CNTs (0.25, 0.5, 0.75, 1 wt%) nanoparticles was probe-sonicated in ethanol solution for 1 h. Simultaneously, ultrasonication of pure Al powder was performed in an ethanol solution. The mixture of BN-CNTs was added dropwise to the Al-ethanol solution and further probe-sonicated for 1 h. Subsequently, the same procedures as discussed above were followed. The detailed schematic diagram of the fabrication of BN-CNTs/Al is shown in Fig. 1.

2.3 Characterization and Testing

The morphology and compositional analysis of the available powders and fabricated sintered specimens were investigated

Table 2 Compositions of fabricated BN/Al and BN-CNTs/Al composites

Composition		h-BN (wt%)	CNTs (wt%)	Al (wt%)
Pure Al	Al	–	–	100
BN/Al Composites	1BN/Al	1	–	99
	3BN/Al	3	–	97
	5BN/Al	5	–	95
	7BN/Al	7	–	93
BN-CNTs/Al Composites	3BN-0.25CNTs/Al	3	0.25	96.75
	3BN-0.5CNTs/Al	3	0.5	96.5
	3BN-0.75CNTs/Al	3	0.75	96.25
	3BN-1CNTs/Al	3	1	96

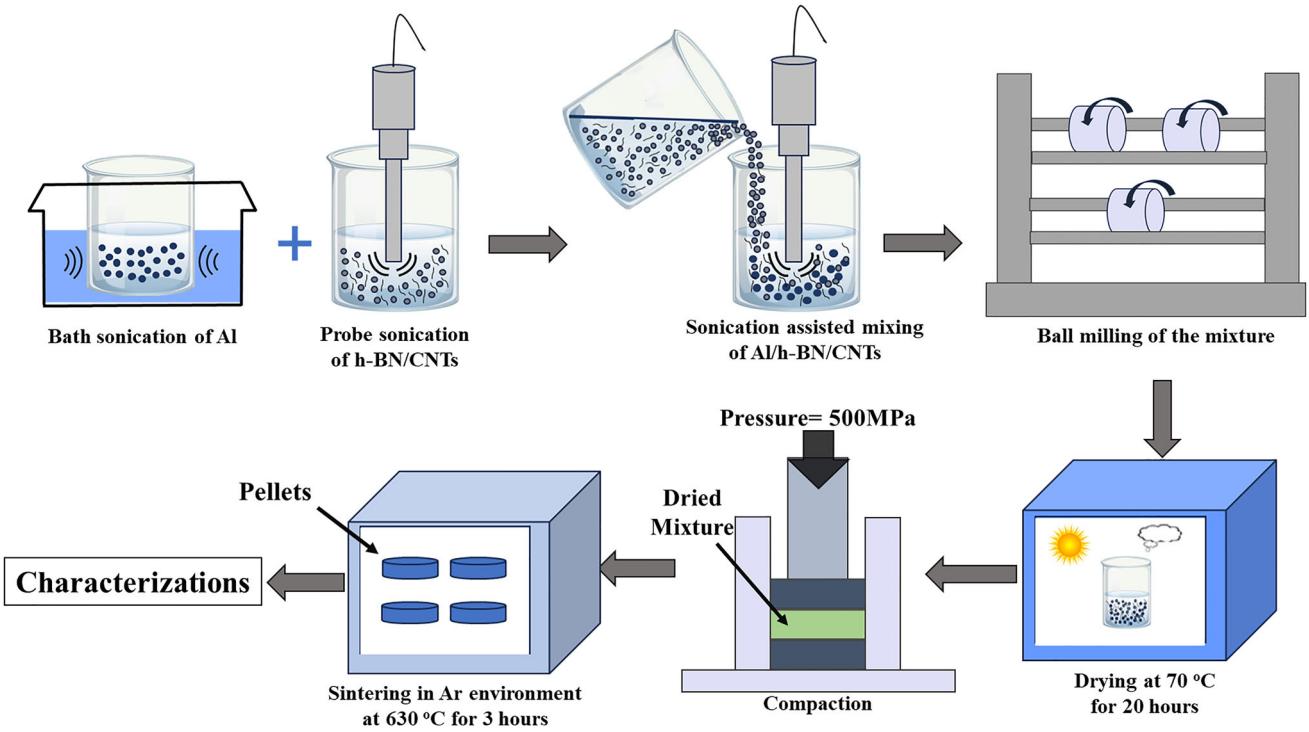

Fig. 1 Schematic diagram of BN-CNTs/Al composites fabricated via PM route

using scanning electron microscopy (Carl Zeiss Evo 15, Germany). X-ray diffraction analysis (Proto Manufacturing Ltd, Canada) was conducted to probe the phase study of prepared samples and powders, scanning at a rate of 2°/min in the angle range of $20^{o} \leq 2\Theta \leq 80°$. Raman spectroscopy (BWTEK, USA) was performed to determine the existence of CNTs structure in composites. Additionally, helium pyrometry (IQIPyc, InstruQuest Inc. Scientific Instruments R&D, USA) was used to measure the green and sintered densities of all the specimens. For Al-BN and Al-3BN-CNTs composites, the theoretical density (ρ_T) and relative densification were calculated using Eq. (1) and (2):

$$1/\text{theoretical } \rho_T = (\%\text{Al}/\rho_{\text{Al}}) + (\%\text{BN}/\rho_{\text{BN}}) + (\%\text{CNTs}/\rho_{\text{CNTs}}) \quad (1)$$

$$\text{Relative densification } (\%) = (\rho_S/\rho_T) \times 100 \quad (2)$$

In Eq. (1), the theoretical densities of Al (2.7 g/cm^3), h-BN (2.3 g/cm^3) and CNTs (1.80 g/cm^3) are represented by ρ_{Al}, ρ_{BN} and ρ_{CNTs}, respectively, while in Eq. (2), ρ_s and ρ_T correspond to the sintered and theoretical density, respectively. Furthermore, the percent porosity ($P\%$) in the composites was determined by the following formula (3).

$$\text{Porosity } \% = (1 - \rho_S/\rho_T) \times 100 \quad (3)$$

In the above formula, ρ_S represents the sintered density and ρ_T represents the theoretical density of the composites.

The specimens' hardness values were measured using Vickers microhardness tester (Tukon-300) with a 3-mm ball

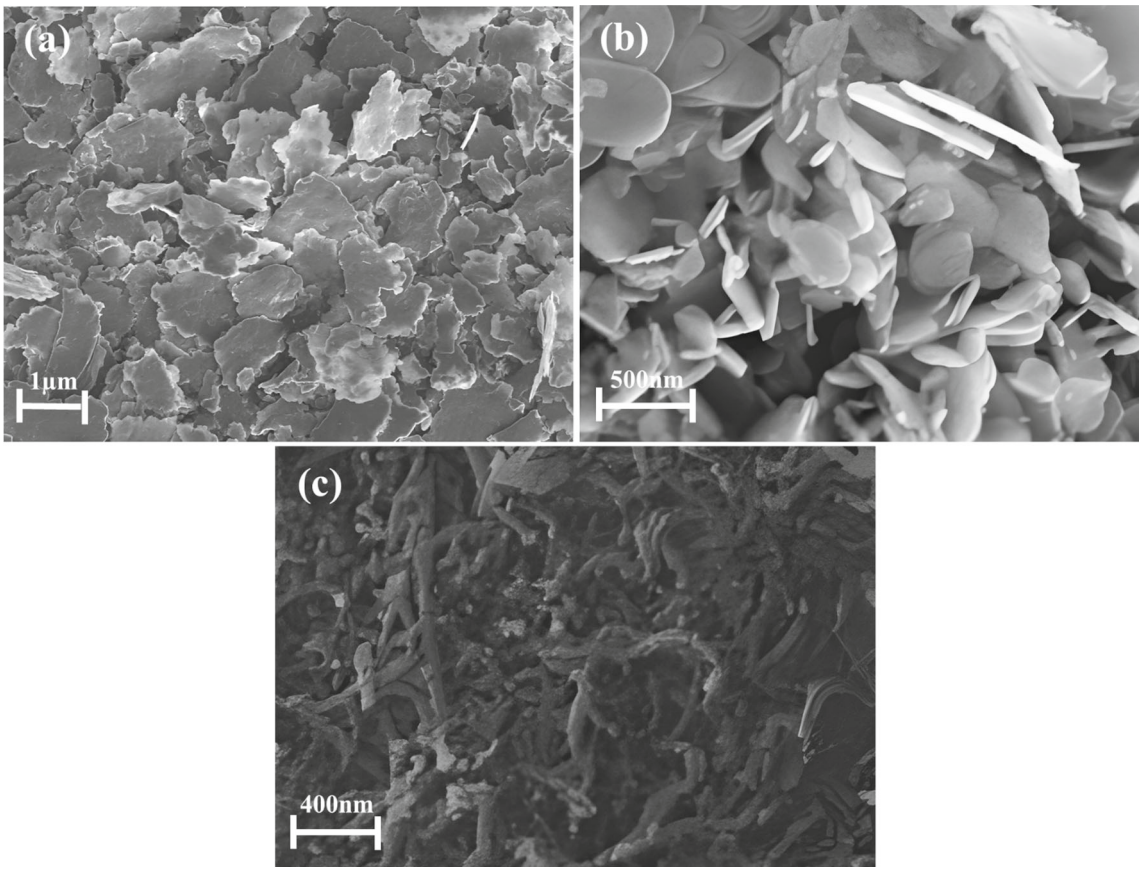

Fig. 2 SEM micrographs of pure **a** Al **b** BN **c** CNTs

indenter, operating at a load of 100 gf and a dwell time of 15 s. The average values obtained from at least ten measurements at the polished surface for distinct areas of each specimen were taken to compute the mean hardness value. The tensile properties of the pure and prepared composites were measured at room temperature using UTM (Instron 5567) operating with a strain rate of 2 mm/s. The ASTM E8 standard was used to prepare dog bone-shaped of rectangular tensile test samples with a gauge length of 20 mm and a width of 5 mm. For DSC analysis, a simultaneous thermal analyzer (STA-8000, PerkinElmer, USA) was used in the temperature range from 30 °C to 1100 °C with a heating rate of 10 °C/min in a nitrogen environment to reduce the effect of oxidation. For this test, samples of ~ 20 mg were cut from sintered pellets.

3 Results and Discussion

3.1 Powder Characterization

The representative morphology of the initial powders observed through SEM is illustrated in Fig. 2. As evident from Fig. 2a, the primary aluminum powder exhibited irregular and flaky morphology. Moreover, h-BN in Fig. 2b indicated a disk-like morphology, while MWCNTs utilized have a clear tube structure and slender shape as presented in Fig. 2c.

To analyze the crystalline phase and planes of pure Al, h-BN and CNTs powders, XRD analysis was performed as shown in Fig. 3. In Fig. 3a, the high-intensity peaks of various crystalline phases of pure aluminum (JCPDS card no: 89–4037) can be clearly depicted at $2\theta = 38°$ (111), 45^{o} (200), 65^{o} (220) and 78^{o} (311). However, XRD peaks

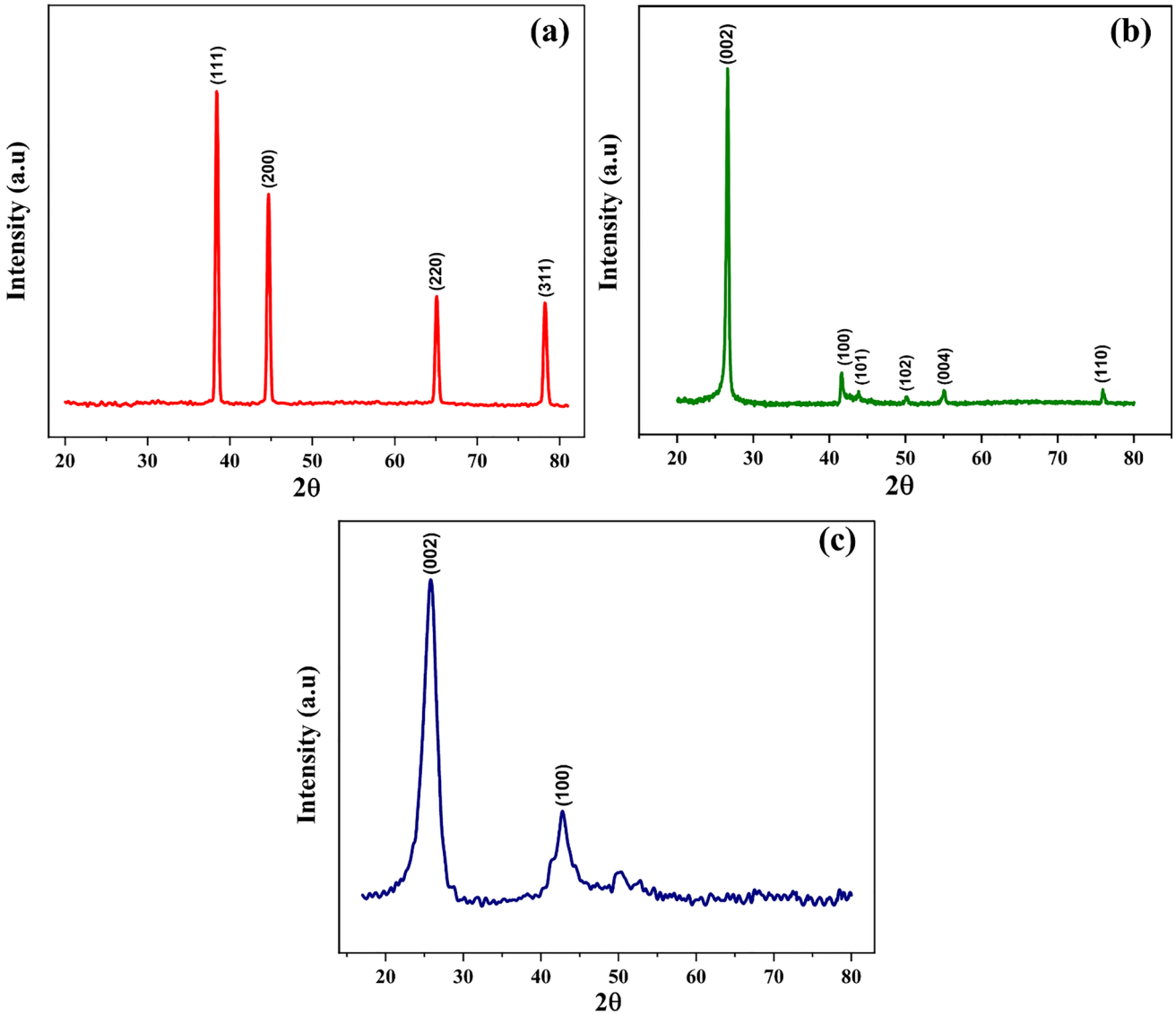

Fig. 3 XRD pattern of pure **a** Al **b** BN **c** CNTs powders

patterns for hexagonal BN with JCPDS card numbers of 85–1068 appeared at 2ϴ = 76°, 55°, 50°, 44° 42° and 28° corresponding to the (110), (004), (102), (101), (100) and (002) planes, respectively (Fig. 3b). As illustrated in Fig. 3c, the crystalline peaks of CNTs (JCPDS card no:75–1621) appeared at approximately 2ϴ = 44.8° and 26.5° corresponding (100) and (002) planes, respectively. Moreover, the peaks that appeared at 2ϴ = ~ 50° were due to the impurity present in CNTs.

3.2 Density and Percent Porosity Results of the Composites

The sintered, theoretical, relative densification and percent porosity of various compositions of BN/Al and BN-CNTs/Al pallets were measured and depicted in Table 3. As indicated in Table 3, it was evident that the incorporation of h-BN in the Al matrix up to a concentration of 3 wt% leads to a gradual increase in relative densification of the BN/Al composite. The highest relative densification and minimum porosity were obtained for the 3BN/Al composite, which was 96.8% and 3.1%, respectively. However, further increase of h-BN content leads to decreased densification, which is because of the presence of porosity, poor wettability of h-BN (as shown in Fig. 4b) and the ability of h-BN to inhibit the rearrangement of particles during sintering [37, 38].

Among all the BN/Al composites, 3BN/Al exhibits the highest density. Therefore, it was preferred to study the effect of CNTs addition (ranging from 0.25 to 1 wt%) on the densification, tensile strength and hardness of Al matrix

Table 3 The theoretical, sintered, relative densification and porosity (%) of BN/Al and 3BN-CNTs/Al composites

Compositions		Theoretical density (g/cm^3)	Sintered Density (g/cm^3)	Relative Densifications (%)	Porosity (%)
Pure Al	Al	2.70	2.54	93.7	6.2
BN/Al Composites	1BN/Al	2.69	2.55	95.5	4.4
	Al-3BN/Al	2.68	2.60	96.8	3.1
	Al-5BN/Al	2.67	2.56	95.1	4.8
	Al-7BN/Al	2.65	2.53	94.7	5.2
BN-CNTs/Al Composites	3BN-0.25CNTs/Al	2.69	2.61	97.0	2.9
	3BN-0.5CNTs/Al	2.69	2.63	97.7	2.2
	3BN-0.75CNTs/Al	2.69	2.59	96.2	3.7
	3BN-1CNTs/Al	2.69	2.57	95.5	4.4

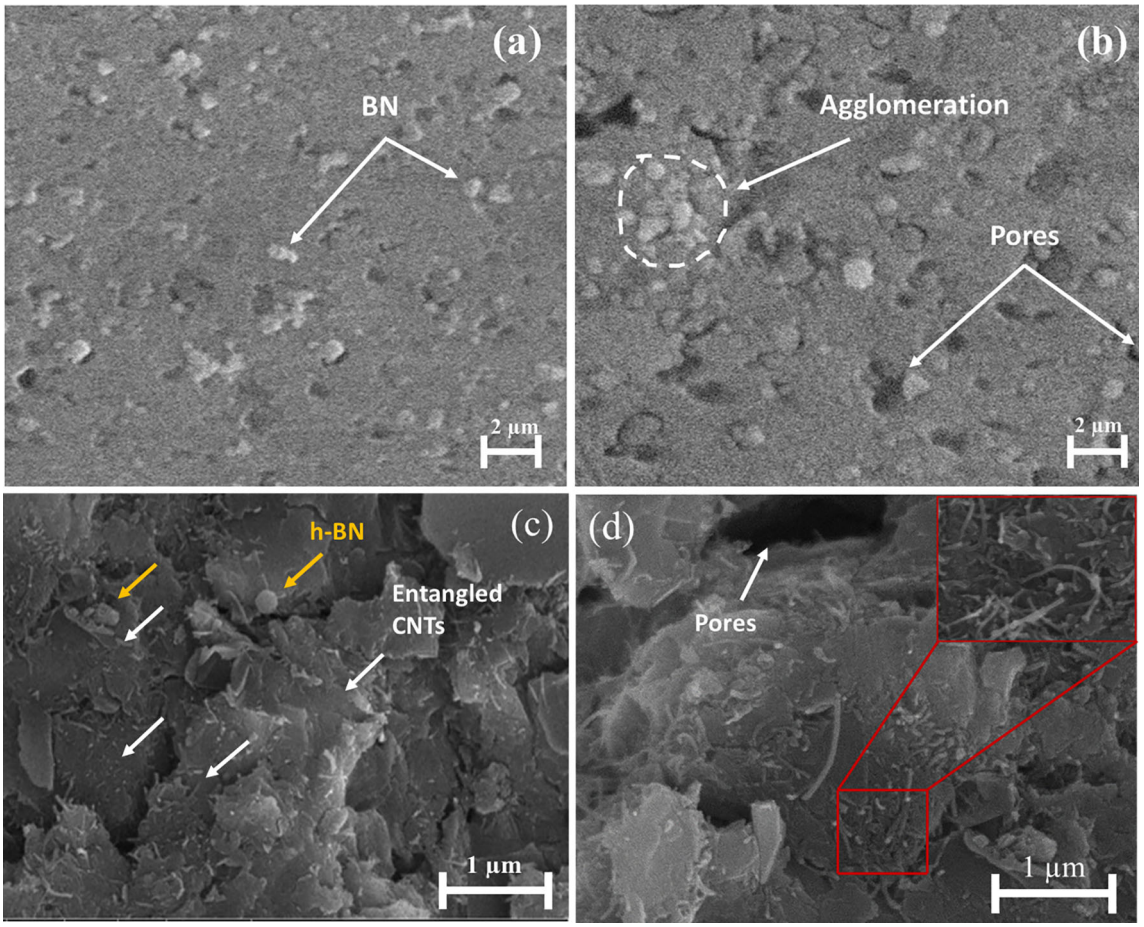

Fig. 4 SEM images of the composites: **a** 3BN/Al **b** 7BN/Al **c** 3BN-0.5CNTs/Al **d** 3BN-1CNTs/Al

composites. As demonstrated in Table 3, the relative densification of the 3BN-CNTs/Al slightly improved at first and then decreased. The composite with 3 wt% h-BN and 0.5 wt% of CNTs showed maximum relative densification with minimum porosity of 97.7 and 2.2% among all the composites, respectively. The reason for better densification was good interfacial bonding and even dispersion of Al, h-BN and CNTs (Fig. 4c and Fig. 11b). On the contrary, CNTs addition of more than 0.5 wt% causes agglomeration which decreases the densification of the composite. The same results were noted by Zhi Liao [39] and Zhou et al. [40] that a higher wt% CNTs content increases porosity and reduces densification due to the clusters of CNTs. Furthermore, the higher addition of CNTs causes the composite's improved wettability

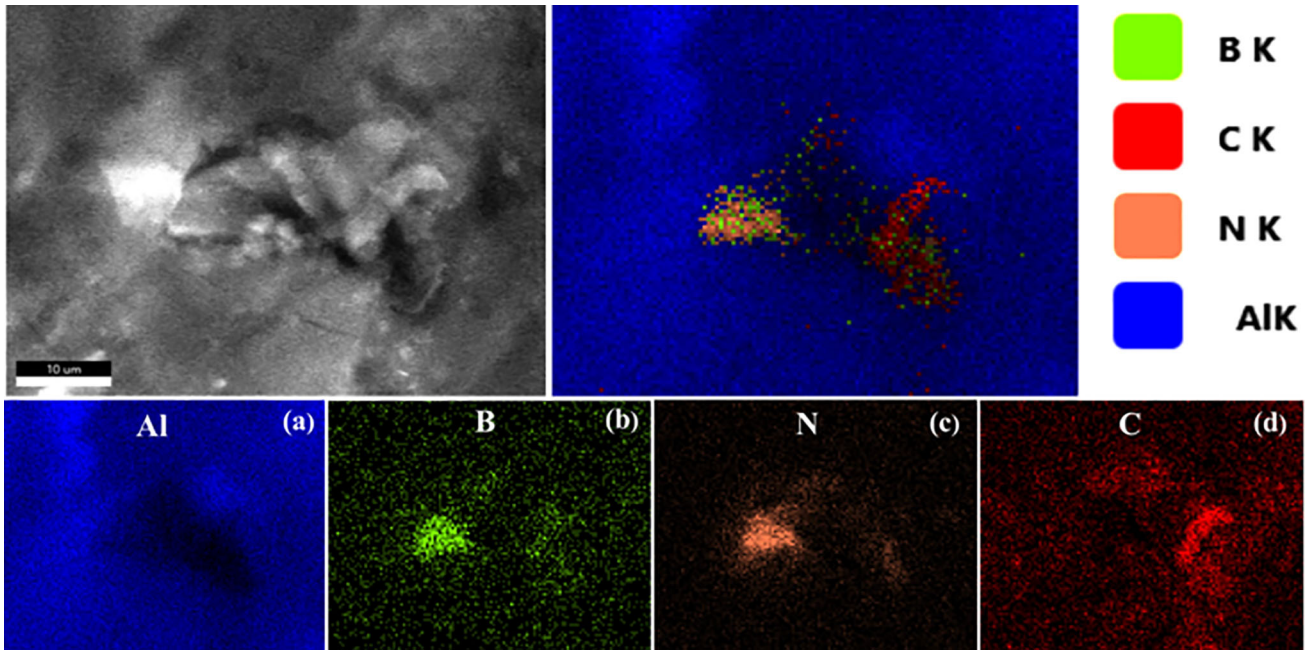

Fig. 5 The SEM-Elemental Mapping images of 3BN-1CNTs/Al **a** Al **b** B **c** N **d** C

through eutectic melting to diminish and the conglomeration of CNTs increases. These factors collectively contributed to the reduced densification of the composites [41].

3.3 Microstructural Analysis via SEM

The micrographs presented provided a detailed examination of the polished surface microstructure of sintered samples. From the micrographs of 3BN/Al as shown in Fig. 4a, it can be observed that h-BN particles were dispersed uniformly in the Al matrix and had a strong neck between the grain boundaries. However, Fig. 4b displays the micrographs of 7BN/Al, which clearly shows the agglomeration of h-BN within the matrix. In this case, there was inadequate dispersion of the reinforcement, causing h-BN to cluster and aggregation which leads to porosity. The presence of porosity in the microstructure of the 7BN/Al composite caused to inferior its physical and mechanical properties.

Moreover, while considering the composites containing MWCNTs, it could be observed that CNTs were entangled between the Al grains and has uniform distribution throughout the matrix without any clustering (Fig. 4c). This even distribution of CNTs within 3BN-0.5CNTs/Al composite makes it more densely packed and well-bonded microstructure with minimal porosity as compared to other composites. Furthermore, the presence of CNTs between the Al grains inhibits the motion of dislocations [32]. As a result, the composite exhibited superior characteristics in terms of relative densification, Vickers hardness and tensile strength. However, as the content of MWCNTs increases more than 0.5 wt% , the tendency for particles to clump together and make agglomerates also increases. This can be observed in Fig. 4d, where clusters of MWCNTs in Al matrix were found due to the electrostatic attractive forces between the reinforcement. The presence of these agglomerated CNTs creates porosity which has a negative impact on the mechanical characteristics of the composite due to the fact that micropores serve as sources of cracks, fracture and various other imperfections.

The SEM elemental mapping analysis of 3BN-0.5CNTs/Al composites was performed to observe the presence and distribution of BN and CNTs in the Al matrix as shown in Fig. 5. From the elemental analysis, the primary materials present in the composite are illustrated in Fig. 5a Al (b) B (c) N (d) C. It can be seen that the distribution of h-BN and CNTs was not uniform and formed clustering of both h-BN and CNTs. The h-BN and CNTs clusters wrap around the Al grain which diminishes their reinforcing action and behaves as a solid lubricant; as a result, materials can easily slide during plastic deformation.

3.4 XRD Analysis

The XRD pattern of 3BN-CNTs/Al composites is presented in Fig. 6. As demonstrated in Fig. 6, it could be seen that the appearance of crystal peaks at $2\theta = 38°, 45°, 65°, 78°$ and $2\theta = 28°, 50°$ and 55° endorses the existence of Al and h-BN in all composites, respectively. Furthermore, the CNTs peaks appeared at 2θ equal to 44.8° and 25° as depicted in Fig. 3c disappeared in Al-BN-CNTs composites after sintering, which could be ascribed to the even dispersion, low

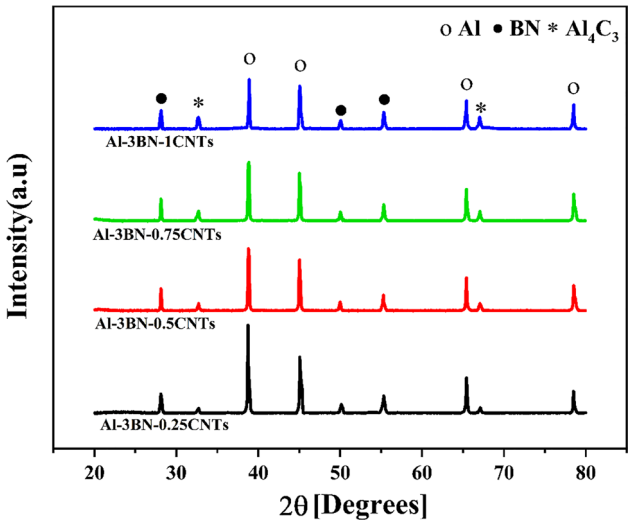

Fig. 6 XRD pattern of pure Al and 3BN-CNTs/Al composites

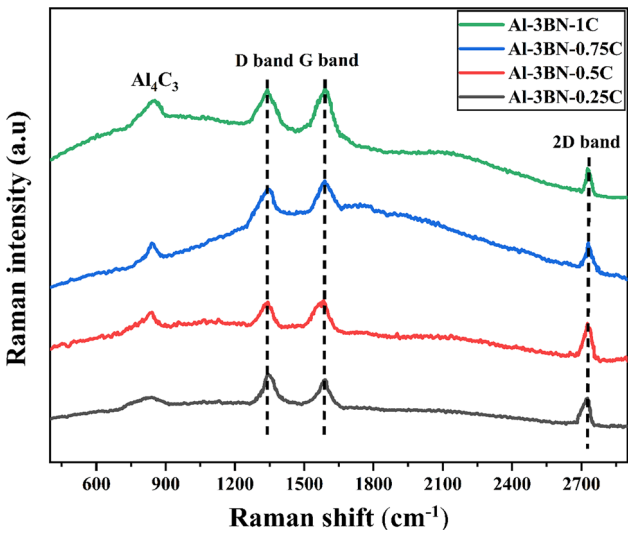

Fig. 7 Raman spectroscopy of 3BN-CNTs/Al composites

amount of CNTs present as well as the small detection limit of XRD. A similar trend was observed by Senel [42] and Yadav [41]. Moreover, several new peaks were observed which correspond to the in situ formed phase of Al_4C_3 in BN-CNTs/Al composites. These peaks are the result of a chemical reaction between the CNTs and the aluminum matrix that may occur at 630 °C during sintering.

3.5 Raman Spectroscopy

Figure 7 displays the Raman spectrum of 3BN-CNTs/Al composites, which confirms the presence of CNTs and the formation of Al_4C_3 phase. The spectra typically exhibit characteristic Al_4C_3 band peaks at approximately 840 cm^{-1}, as well as D-band peaks at ~ 1340 cm^{-1}, which correspond

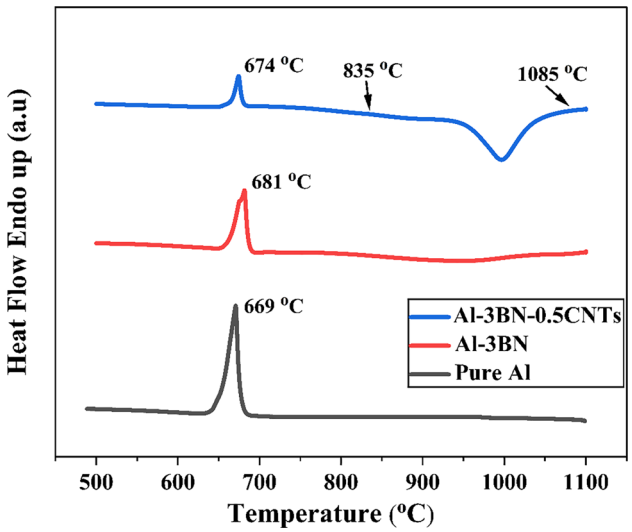

Fig. 8 DSC curves of **a** Pure Al **b** 3BN/Al **c** 3BN-0.5CNTs/Al

to the defective planes of the CNTs, G-band peaks at ~ 1590 cm^{-1}, which are associated with graphite and 2D band at ~ 2727 cm^{-1} [43–45].

3.6 Thermal Analysis via DSC

The DSC curves of the pure Al and 3BN-0.5CNTs/Al composite are depicted in Fig. 8. It is apparent that the DSC curve of pure Al and Al-3BN reveals only an endothermic peak, whereas the DSC result for the BN-CNTs/Al composite discloses both an exothermic peak (at 835–1085 °C) alongside the endothermic peak compared to the DSC result of pure Al. It is evident that the endothermic peak that appeared at 674 °C represents the melting point of pure Al, while the exothermic peak may correspond to the reaction peak between Al and CNTs [33, 46].

In the present study, carbon nanotubes are used to reinforce the Al matrix rather than graphite. Due to the lack of prism planes in CNTs, the carbide formation is restricted at the interface of Al/CNTs. The carbide formation and growth have only been observed in graphitic structure along the reactive prismatic planes {1 0–1 0}, which are absent in CNTs [46–48]. However, CVD-grown carbon nanotubes typically exhibit a few flaws and a considerable amorphous carbon coating on the surface of the tube, which indicates that certain graphitic prism planes are in contact with aluminum when CNTs are employed as reinforcement. Also, it is important to note that the CNTs used in this study have small diameters and larger lengths, providing large surface areas that may have contributed to the enhanced probability of a reaction between the CNTs and the aluminum matrix. The buildup of an amorphous carbon layer along with the existence of defects will facilitate the precipitation of Al_4C_3 [47,

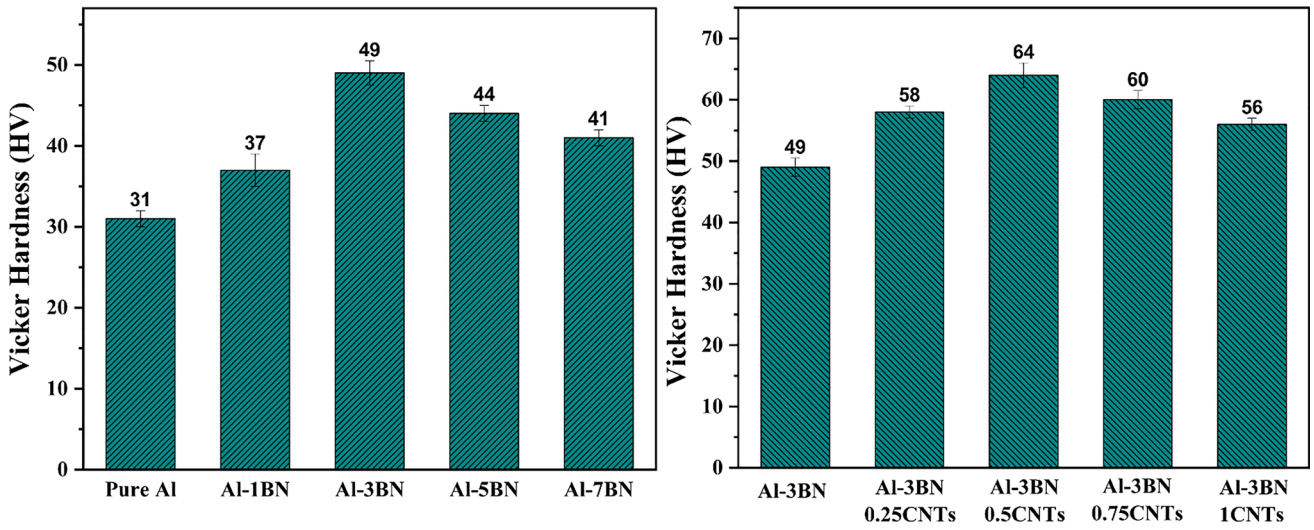

Fig. 9 The micro-Vickers hardness for **a** 3BN/Al **b** 3BN-CNT/Al

49]. According to Lijie Ci et al. [47], the interfacial interaction between the Al layers and CNTs was enhanced by the formation of carbide on the surface of the CNTs and thus will increase the load transfer efficiency, which further contributes to improving the composite's mechanical properties. For Al and CNTs, a strong transition interface is required to form a strong bond. The strong bonding at the interface depends upon the wettability of the Al and CNTs, which is usually weak because of the difference in surface energy. Therefore, the bonding was significantly improved as a result of the formation of Al_4C_3 via interfacial chemical reaction. This improvement is due to the in situ produced carbides which not only enhance the wettability, but it also contributes to bind the CNTs during plastic deformation.

3.7 Microhardness Evaluations

Micro-Vickers hardness variations of pure Al, BN/Al and BN-CNTs/Al composites are presented in Fig. 9. The results show that the inclusion of h-BN in the Al matrix significantly improved the microhardness from 31 ± 1 to 49 ± 1.5 HV as BN content increased from 0 to 3wt% in Fig. 9a. The highest microhardness up to 3 wt% BN was manifested by better distribution and higher hardness of h-BN than pure Al. Thus, the composite's hardness is significantly improved by the incorporation of BN into the Al matrix.

Moreover, Fig. 9b illustrates the influence of CNTs addition (ranging from 0 to 1wt%) to 3BN/Al composition on the microhardness of BN-CNTs/Al composite. It could be seen that the hardness was enhanced from 49 ± 1.5 to 58 ± 2 by addition of 0.25 wt% of CNTs (87% increment as compared to pure Al). Further inclusion of 0.5wt% of CNTs to Al-3BN composite improved the hardness to 64 ± 2, which was about 30.6% and 106.4% increment as compared to 3BN/Al and pure Al, respectively. This enhancement in microhardness was mainly ascribed to homogeneous dispersion, high surface area of CNTs and strong adhesion between the reinforcements and matrix (as can be seen in Fig. 4c and Fig. 11b). In addition, the inclusion of CNTs in the Al matrix enhanced the dislocation density attributed to the nano-size structure of CNTs. This increase in the density of dislocation improved the BN-GNPs/Al composites' hardness [50]. However, a decline in hardness was observed with further loading of CNTs content (from 0.5 to 1 wt%), which can be attributed to the agglomeration of CNTs (as depicted in Fig. 4d) which had an adverse effect on densification, wettability and the efficient transfer of load to the reinforcements [41].

3.8 Mechanical Strength Evaluations

Figure 10 illustrates the plot of tensile strength of the pure Al and 3BN-CNTs/Al composites. A positive and significant effect was observed on the tensile strength values of the composites as the concentration of CNTs increased. It was noted that pure Al exhibited a tensile strength of 83 MPa, which closely aligns with the average tensile strength value reported by [42]. This alignment provides additional confirmation for the accuracy of the model employed for predicting the tensile strength of the composite. The introduction of 1wt% of CNTs to 3BN/Al composite enhanced the tensile strength by 149. 3% as compared to pure Al. Further addition of 0.5 wt% of CNTs recorded a maximum tensile strength of 240 MPa, making a significant increment of 189.1% as compared to pure Al (83 MPa). This finding suggests that 3 wt% of h-BN and 0.5 wt% of CNTs were the optimal amount of reinforcements in the Al matrix for achieving maximum

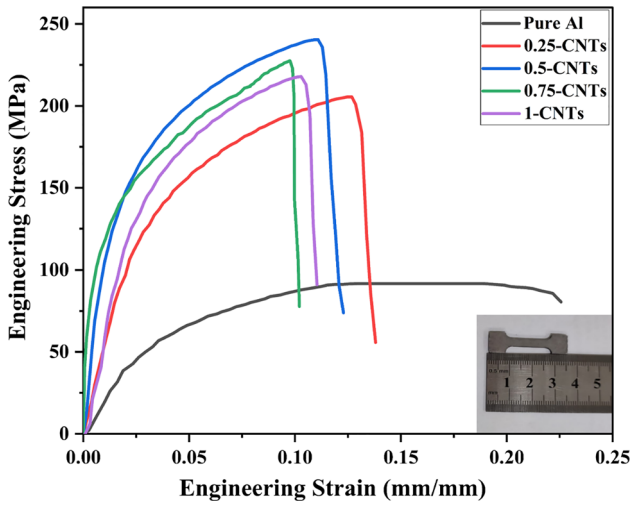

Fig. 10 The tensile strength for pure Al and Al-3BN-CNTs composites

mechanical strength. Usually, the improvement in mechanical properties with the inclusion of CNTs can be described by fundamental strengthening mechanisms such as load transfer mechanism [51], grain refinement [52], thermal expansion mismatch between reinforcement matrix [53] and Orowan strengthening [54]. In the present work, the increment in tensile strength could be attributed to (i) load transfer from the matrix to the reinforcements (h-BN and CNTs) through the interface during plastic deformation. This was because of the equal distribution of reinforcement particles, strong adhesion between the reinforcements/matrix interface and better densification (97.3%) of 3BN-0.5CNTs/Al composite through optimal sintering parameters (Fig. 4c and Fig. 11b). (ii) The formation of Al_4C_3 phase by a partially chemical reaction of Al and CNTs (as confirmed from the XRD, DSC and Raman) also improved load transfer efficiency through the interface [33, 47]. (iii) A significant mismatch of thermal expansion (CTE) between the Al (23.6×10^{-6} K^{-1}) and CNTs (1×10^{-6} K^{-1}). This apparent mismatch in the thermal expansion coefficient between the Al matrix and the CNTs causes prismatic punching of dislocation at the interface which contributes to the work hardening of the matrix [53]. There will likely be higher dislocation density, which would contribute to more strengthening. However, above 0.5 wt% CNTs addition dropped the tensile strength due to the clusters of CNTs which stimulate porosity and prevent effective bonding between the Al matrix and CNTs (Fig. 4d). Moreover, these agglomerated MWCNTs weaken the grain boundaries and make the composite incapable of effectively transferring or distributing stress, but they also served as

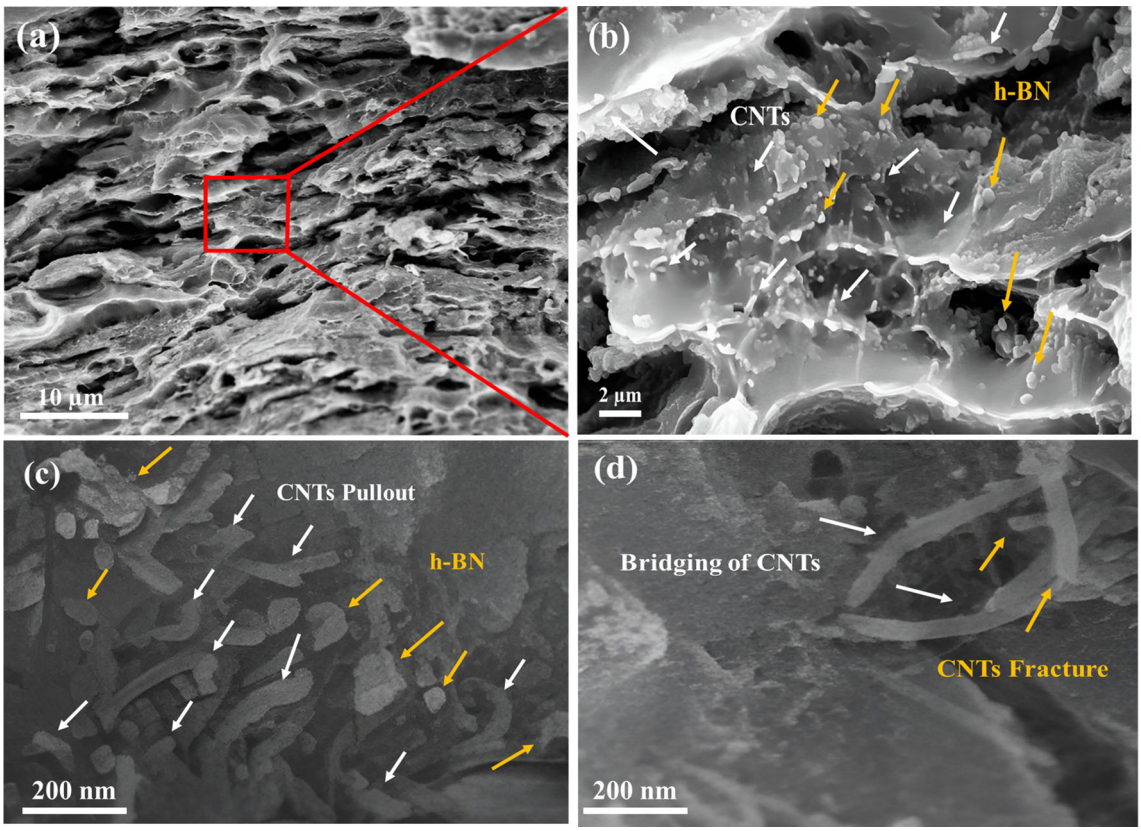

Fig. 11 SEM micrographs of the fractured surface of Al-3BN-0.5CNTs composite: **a** Layered structure of composite **b** Strong neck and well-bonded structure **c** Pullout of CNTs **d** Fracture and Bridging of CNTs

sources of cracks and fracture which depreciated the mechanical strength of the composite. This observation agreed with the findings reported by Lewandowski and Dutton [55], and a similar trend was noted by Maiti et al. [56].

3.9 Fractography Analysis

Figure 11a–d shows the low- and high-magnification fracture surface morphologies of 3BN-0.5CNTs/Al composites after the tensile test. In Fig. 11a, a ductile–brittle mixed fracture mode could be seen from the fracture surface of the specimen. From Fig. 11b, it could be noted that h-BN and CNTs are pulled out from the fracture surface and evenly distributed in Al matrix. Moreover, few dimples can be observed on the fracture surface, indicating a moderate level of plasticity in the 3BN-0.5CNTs/Al composites (Fig. 11b). In addition, CNTs with tubular structure can be observed, which are embedded and uniformly distributed throughout the matrix, and some CNTs pulled out are perpendicular to the fracture surface (Fig. 11c). This implies that, during tensile loading, the strong interfacial bonding between CNTs and Al through a partial chemical reaction was achieved, which facilitates the efficient transfer of load from the matrix to the reinforcements (h-BN and CNTs) [57]. Furthermore, CNTs fracture and bridging were also observed between the fracture surface of the aluminum matrix, which serves to transfer the stress within the composite to improve the composite's mechanical properties. These findings are in good agreement with the study conducted by Noguchi [58] and Chunfeng [59].

4 Conclusions

In the present study, various reinforcing contents of BN-reinforced (1,3,5,7 wt%) and CNTs-reinforced (0.25, 0.5, 0.75, 1 wt. %) synergistic Al matrix composites were fabricated through powder metallurgy route. The effect of pure h-BN and binary h-BN-CNTs addition on the microstructure, density, Vickers hardness and ultimate tensile strength of Al matrix composite was evaluated. The experimental results showed the highest relative densification (96.8%), low porosity (3.1%) and Vickers hardness (49 $\pm$ 1.5 HV) values were obtained for 3BN/Al composites. Among all the tested composites, the 3BN/Al composite exhibited superior properties and was therefore selected for further investigation for synergistic effects of CNTs on the mechanical strength of Al-3BN-CNTs composites. And among the hybrid composites, the 3BN-0.5CNTs/Al gave better mechanical properties, including the highest relative densification (97.7%), UTS (240 MPa), Vickers hardness (64 $\pm$ 2 HV) and low porosity (2.2%). This improvement in UTS and Vickers hardness of the composite was about 189% and 106% to that of the pure Al, respectively. The reason for better mechanical strength was ascribed to well distribution of reinforcements (h-BN, CNTs), and the presence of reinforcement between the Al grain acts as an obstacle which inhibits the movement of dislocation. In addition, the CNTs pullout, bridging and formation of Al_4C_3 phase are responsible for efficient load transfer which in turn led to significantly enhanced mechanical properties of the composites. However, the mechanical strength of composites depreciated at higher loading of CNTs ($\geq$ 0.5 wt%) and h-BN ($\geq$ 3 wt%) due to the agglomeration of BN and CNTs nanoparticles. The results showed the binary h-BN and CNTs have a synergistic effect on the mechanical strength of Al matrix composites. The superior mechanical properties exhibited by BN-CNTs/Al composites make them favorable as structural and functional materials for aerospace and automobile industries.

Acknowledgements The authors acknowledge Higher Education Commission (HEC) of Pakistan for providing the financial assistance to carry out this research work via Project No. HEC-NRPU # 10493.

Author contributions The synthesis and microstructural analysis of the composites and preparation of the initial manuscript draft were done by Muhammad Awais Khan. The thermal analysis and mechanical characterization were done by Atteeq Uz Zaman. Muhammad Ramzan Abdul Karim designed and supervised the research project and reviewed, edited and finalized the manuscript. Azhar Hussain helped with XRD analysis and fractography analysis. Ehsan Ul Haq helped with the Raman analysis and proofreading of the manuscript. All authors reviewed and approved the final draft of the manuscript.

Declarations

Conflict of interest All the authors declare that there are no conflicts of financial or any other competing interests.

References

1. Bhoi, N.K.; Singh, H.; Pratap, S.: Developments in the aluminum metal matrix composites reinforced by micro/nano particles—A review. J. Compos. Mater. **54**(6), 813–833 (2020). https://doi.org/10.1177/0021998319865307
2. Sharma, D.K.; Mahant, D.; Upadhyay, G.: Manufacturing of metal matrix composites: a state of review. Mater. Today Proc. **26**, 506–519 (2019). https://doi.org/10.1016/j.matpr.2019.12.128
3. Sahin, Y.; Murphy, S.: The effect of fibre orientation of the dry sliding wear of borsic-reinforced 2014 aluminium alloy. J. Mater. Sci. **31**(20), 5399–5407 (1996). https://doi.org/10.1007/BF01159309
4. Hanumanth, G.S.; Irons, G.A.: Particle incorporation by melt stirring for the production of metal-matrix composites. J. Mater. Sci. **28**(9), 2459–2465 (1993). https://doi.org/10.1007/BF01151680
5. K. K. Chawla, 2012 "Metal Matrix Composites," *Compos. Mater.*, doi: https://doi.org/10.1007/978-0-387-74365-3_6.
6. Koli, D.K.; Agnihotri, G.; Purohit, R.: Advanced aluminium matrix composites: the critical need of automotive and aerospace engineering fields. Mater. Today Proc. **2**(4–5), 3032–3041 (2015). https://doi.org/10.1016/J.MATPR.2015.07.290
7. Hussain, G.; Hashemi, R.; Hashemi, H.; Al-Ghamdi, K.A.: An experimental study on multi-pass friction stir processing of Al/TiN

composite: some microstructural, mechanical, and wear characteristics. Int. J. Adv. Manuf. Technol. **84**(1–4), 533–546 (2016). https://doi.org/10.1007/S00170-015-7504-5/METRICS
8. Firestein, K.L., et al.: Fabrication, characterization, and mechanical properties of spark plasma sintered Al-BN nanoparticle composites. Mater. Sci. Eng. A **642**, 104–112 (2015). https://doi.org/10.1016/j.msea.2015.06.059
9. Mohanavel, V.; Ravichandran, M.: Experimental investigation on mechanical properties of AA7075-AlN composites. Mater. Test. **61**(6), 554–558 (2019). https://doi.org/10.3139/120.111354/MACHINEREADABLECITATION/RIS
10. A. U. Zaman *et al.:* Tape Casting and Characterization of h-BN / PU Composite Coatings for Corrosion Resistance Applications. Dig. Man. Tech., 156–163 (2023). https://doi.org/10.37256/dmt.3220233092
11. Penchal Reddy, M., et al.: Enhancing compressive, tensile, thermal and damping response of pure Al using BN nanoparticles. J. Alloys Compd. **762**, 398–408 (2018). https://doi.org/10.1016/J.JALLCOM.2018.05.205
12. Gostariani, R.; Ebrahimi, R.; Asadi, M.; Mohammad, A.; Paydar, H.: Mechanical properties of Al / BN nanocomposites fabricated by planetary ball milling and conventional hot extrusion. Acta Metall. Sin. English Lett. **31**(3), 245–253 (2018). https://doi.org/10.1007/s40195-017-0640-1
13. Gopinath, S.; Prince, M.; Raghav, G.R.: Enhancing the mechanical, wear and corrosion behaviour of stir casted aluminium 6061 hybrid composites through the incorporation of boron nitride and aluminium oxide particles. Mater. Res. Express **7**, 1 (2020). https://doi.org/10.1088/2053-1591/ab6c1d
14. Abdul Karim, M.R.; Khan, M.A.; Zaman, A.U.; Hussain, A.: Hexagonal boron nitride-based composites: an overview of processing approaches and mechanical properties. J. Korean Ceram. Soc. **2022**, 1–23 (2022). https://doi.org/10.1007/S43207-022-00251-8
15. Bakshi, S.R.; Lahiri, D.; Agarwal, A.: Carbon nanotube reinforced metal matrix composites - a review. Int. Mater. Rev. **55**(1), 41–64 (2013). https://doi.org/10.1179/095066009X12572530170543
16. Tjong, S.C.: Recent progress in the development and properties of novel metal matrix nanocomposites reinforced with carbon nanotubes and graphene nanosheets. Mater. Sci. Eng. R. Rep. **74**(10), 281–350 (2013). https://doi.org/10.1016/J.MSER.2013.08.001
17. Krishnan, A.; Dujardin, E.; Ebbesen, T.W.; Yianilos, P.N.; Treacy, M.M.J.: Young's modulus of single-walled nanotubes. Phys. Rev. B **58**(20), 14013 (1998). https://doi.org/10.1103/PhysRevB.58.14013
18. Kwon, Y.K.; Kim, P.: Unusually high thermal conductivity in carbon nanotubes. High Therm. Conduct. Mater. (2006). https://doi.org/10.1007/0-387-25100-6_8/COVER
19. Dorri Moghadam, A.; Omrani, E.; Menezes, P.L.; Rohatgi, P.K.: Mechanical and tribological properties of self-lubricating metal matrix nanocomposites reinforced by carbon nanotubes (CNTs) and graphene – A review. Compos. Part B Eng. **77**, 402–420 (2015). https://doi.org/10.1016/J.COMPOSITESB.2015.03.014
20. Yu, M.F.; Lourie, O.; Dyer, M.J.; Moloni, K.; Kelly, T.F.; Ruoff, R.S.: Strength and breaking mechanism of multiwalled carbon nanotubes under tensile load. Science **287**(5453), 637–640 (2000). https://doi.org/10.1126/SCIENCE.287.5453.637/SUPPL_FILE/1046083C1.GIF
21. Bach, L.X.; Son, D.L.; Phong, M.T.; Thang, L.V.; Bian, M.Z.; Nam, N.D.: A study on Mg and AlN composite in microstructural and electrochemical characterizations of extruded aluminum alloy. Compos. Part B Eng. **156**, 332–343 (2019). https://doi.org/10.1016/j.compositesb.2018.08.139
22. Vinayagam, M.: "Synthesis and evaluation on mechanical properties of LM4/AlN alloy based composites." Energy Sources Part A Recover. Util. Environ. Eff. **44**(1), 1888–1897 (2022). https://doi.org/10.1080/15567036.2019.1647313
23. Kumar, S.D.; Ravichandran, M.; Jeevika, A.; Stalin, B.; Kailasanathan, C.; Karthick, A.: Effect of ZrB2 on microstructural, mechanical and corrosion behaviour of aluminium (AA7178) alloy matrix composite prepared by the stir casting route. Ceram. Int. **47**(9), 12951–12962 (2021). https://doi.org/10.1016/j.ceramint.2021.01.158
24. Vithal, D.N.; Krishna, B.B.; Krishna, G.M.: Microstructure, mechanical properties and fracture mechanisms of ZrB2 ceramic reinforced A7075 composites fabricated by stir casting. Mater. Today Commun. **25**, 101289 (2020). https://doi.org/10.1016/j.mtcomm.2020.101289
25. Bandil, K., et al.: Microstructural, mechanical and corrosion behaviour of Al–Si alloy reinforced with SiC metal matrix composite. J. Compos. Mater. **53**(28–30), 4215–4223 (2019). https://doi.org/10.1177/0021998319856679
26. Rahman, M.H.; Al Rashed, H.M.M.: Characterization of silicon carbide reinforced aluminum matrix Composites. Procedia Eng. **90**, 103–109 (2014). https://doi.org/10.1016/j.proeng.2014.11.821
27. James, S.J.; Ganesan, M.; Santhamoorthy, P.; Kuppan, P.: Development of hybrid aluminium metal matrix composite and study of property. Mater. Today Proc. **5**(5), 13048–13054 (2018). https://doi.org/10.1016/j.matpr.2018.02.291
28. Pal, K.; Navin, K.; Kurchania, R.: Study of structural and mechanical behaviour of Al-ZrO2 metal matrix nanocomposites prepared by powder metallurgy method. Mater. Today Proc. **26**, 2714–2719 (2019). https://doi.org/10.1016/j.matpr.2020.02.570
29. Ahmed, H.M.; Ahmed, H.A.; Hefni, M.; Moustafa, E.B.: Effect of grain refinement on the dynamic, mechanical properties, and corrosion behaviour of Al-Mg alloy. Metals **11**(11), 1825 (2021)
30. Kaygısız, Y.; Kayan, D.B.: Effect of heat treatment on the mechanical properties and corrosion behaviour of Al–Si–Mg alloy systems. Phys. Met. Metallogr.Metallogr. **123**(14), 1499–1508 (2022). https://doi.org/10.1134/S0031918X22100210
31. Boesl, B.; Lahiri, D.; Behdad, S.; Agarwal, A.: Direct observation of carbon nanotube induced strengthening in aluminum composite via in situ tensile tests. Carbon N. Y. **69**, 79–85 (2014). https://doi.org/10.1016/j.carbon.2013.11.061
32. Pérez-Bustamante, R., et al.: Microstructural and mechanical characterization of Al-MWCNT composites produced by mechanical milling. Mater. Sci. Eng. A **502**(1–2), 159–163 (2009). https://doi.org/10.1016/j.msea.2008.10.047
33. He, C.N.; Zhao, N.Q.; Shi, C.S.; Song, S.Z.: Mechanical properties and microstructures of carbon nanotube-reinforced Al matrix composite fabricated by in situ chemical vapor deposition. J. Alloys Compd. **487**(1–2), 258–262 (2009). https://doi.org/10.1016/j.jallcom.2009.07.099
34. Guo, B., et al.: Microstructures and mechanical properties of carbon nanotubes reinforced pure aluminum composites synthesized by spark plasma sintering and hot rolling. Mater. Sci. Eng. A **698**(May), 282–288 (2017). https://doi.org/10.1016/j.msea.2017.05.068
35. Zhang, X.; Li, S.; Pan, D.; Pan, B.; Kondoh, K.: Microstructure and synergistic-strengthening efficiency of CNTs-SiCp dual-nano reinforcements in aluminum matrix composites. Compos. Part A Appl. Sci. Manuf. **105**, 87–96 (2018). https://doi.org/10.1016/j.compositesa.2017.11.013
36. Gostariani, R.; Ebrahimi, R.; Asadabad, M.A.; Paydar, M.H.: Mechanical properties of Al/BN nanocomposites fabricated by planetary ball milling and conventional hot extrusion. Acta Metall. Sin. English Lett. **31**(3), 245–253 (2018). https://doi.org/10.1007/S40195-017-0640-1
37. Suryanarayana, C.: Mechanical alloying and milling. Prog. Mater. Sci.. Mater. Sci. **46**(1–2), 1–184 (2001). https://doi.org/10.1016/S0079-6425(99)00010-9

38. Pillari, L.K.; Umasankar, V.; Elamathi, P.; Chandrasekar, G.: Synthesis and characterization of nano hexagonal boron nitride powder and evaluating the influence on aluminium alloy matrix. Mater. Today Proc. **3**(6), 2018–2026 (2016). https://doi.org/10.1016/J.MATPR.2016.04.104
39. Zhi Liao, J.; Tan, M.J.; Sridhar, I.: Spark plasma sintered multi-wall carbon nanotube reinforced aluminum matrix composites. Mater. Des. **31**(1), S96–S100 (2010). https://doi.org/10.1016/j.matdes.2009.10.022
40. Zhou, M., et al.: The effects of carbon nanotubes on the mechanical and wear properties of AZ31 alloy. Materials (Basel) (2017). https://doi.org/10.3390/ma10121385
41. Yadav, V.; Harimkar, S.P.: Microstructure and properties of spark plasma sintered carbon nanotube reinforced aluminum matrix composites. Adv. Eng. Mater. **13**(12), 1128–1134 (2011). https://doi.org/10.1002/adem.201100132
42. Şenel, M.C.; Gürbüz, M.: Synergistic effect of graphene/boron nitride binary nanoparticles on aluminum hybrid composite properties. Adv. Compos. Hybrid Mater. **4**(4), 1248–1260 (2021). https://doi.org/10.1007/S42114-021-00209-0
43. Chen, B., et al.: Solid-state interfacial reaction and load transfer efficiency in carbon nanotubes (CNTs)-reinforced aluminum matrix composites. Carbon N. Y. **114**, 198–208 (2017). https://doi.org/10.1016/j.carbon.2016.12.013
44. Guo, B.; Song, M.; Yi, J.; Ni, S.; Shen, T.; Du, Y.: Improving the mechanical properties of carbon nanotubes reinforced pure aluminum matrix composites by achieving non-equilibrium interface. Mater. Des. **120**, 56–65 (2017). https://doi.org/10.1016/j.matdes.2017.01.096
45. Chen, B.; Kondoh, K.; Imai, H.; Umeda, J.; Takahashi, M.: Simultaneously enhancing strength and ductility of carbon nanotube/aluminum composites by improving bonding conditions. Scr. Mater. **113**, 158–162 (2016). https://doi.org/10.1016/j.scriptamat.2015.11.011
46. Deng, C.F.; Zhang, X.X.; Wang, D.Z.; Ma, Y.X.: Calorimetric study of carbon nanotubes and aluminum. Mater. Lett. **61**(14–15), 3221–3223 (2007). https://doi.org/10.1016/j.matlet.2006.11.037
47. Ci, L.; Ryu, Z.; Jin-Phillipp, N.Y.; Rühle, M.: Investigation of the interfacial reaction between multi-walled carbon nanotubes and aluminum. Acta Mater. Mater. **54**(20), 5367–5375 (2006). https://doi.org/10.1016/j.actamat.2006.06.031
48. Kuzumaki, T.; Miyazawa, K.; Ichinose, H.; Ito, K.: Processing of carbon nanotube reinforced aluminum composite. J. Mater. Res. **13**(9), 2445–2449 (1998). https://doi.org/10.1557/JMR.1998.0340
49. Khalid, F.A.; Beffort, O.; Klotz, U.E.; Keller, B.A.; Gasser, P.; Vaucher, S.: Study of microstructure and interfaces in an aluminium–C60 composite material. Acta Mater. Mater. **51**(15), 4575–4582 (2003). https://doi.org/10.1016/S1359-6454(03)00294-5
50. Paupler, P.; Dieter, G.E.: Mechanical Metallurgy. McGraw-Hill, London (1961)
51. Kelly, A.; Tyson, W.R.: Tensile properties of fibre-reinforced metals: Copper/tungsten and copper/molybdenum. J. Mech. Phys. Solids **13**(6), 329–350 (1965). https://doi.org/10.1016/0022-5096(65)90035-9
52. Mokdad, F.; Chen, D.L.; Liu, Z.Y.; Xiao, B.L.; Ni, D.R.; Ma, Z.Y.: Deformation and strengthening mechanisms of a carbon nanotube reinforced aluminum composite. Carbon N. Y. **104**, 64–77 (2016). https://doi.org/10.1016/j.carbon.2016.03.038
53. George, R.; Kashyap, K.T.; Rahul, R.; Yamdagni, S.: Strengthening in carbon nanotube/aluminium (CNT/Al) composites. Scr. Mater. **53**(10), 1159–1163 (2005). https://doi.org/10.1016/j.scriptamat.2005.07.022
54. Zhang, Z.; Chen, D.L.: Consideration of Orowan strengthening effect in particulate-reinforced metal matrix nanocomposites: A model for predicting their yield strength. Scr. Mater. **54**(7), 1321–1326 (2006). https://doi.org/10.1016/J.SCRIPTAMAT.2005.12.017
55. Lewandowski, J.J.; Liu, C.; Hunt, W.H.: Effects of matrix microstructure and particle distribution on fracture of an aluminum metal matrix composite. Mater. Sci. Eng. A **107**, 241–255 (1989). https://doi.org/10.1016/0921-5093(89)90392-4
56. Peng, H., et al.: Study of distribution of Carbon nanotube in Al-CNT nanocomposite synthesized via Spark-Plasma sintering. Conf. Ser. Mater. Sci. Eng. (2018). https://doi.org/10.1088/1757-899X/338/1/012014
57. Chen, B.; Li, S.; Imai, H.; Jia, L.; Umeda, J.; Takahashi, M.: Load transfer strengthening in carbon nanotubes reinforced metal matrix composites via in-situ tensile tests. Compos. Sci. Technol. **113**, 1–8 (2015). https://doi.org/10.1016/j.compscitech.2015.03.009
58. Noguchi, T.; Magario, A.; Fukazawa, S.; Shimizu, S.; Beppu, J.; Seki, M.: Carbon nanotube/aluminium composites with uniform dispersion. Mater. Trans. **45**(2), 602–604 (2004). https://doi.org/10.2320/matertrans.45.602
59. Deng, C.; Zhang, X.; Ma, Y.; Wang, D.: Fabrication of aluminum matrix composite reinforced with carbon nanotubes. Rare Met. **26**(5), 450–455 (2007). https://doi.org/10.1016/S1001-0521(07)60244-7